J Mater Sci (2007) 42:9504–9510
DOI 10.1007/s10853-007-1956-4

INTERFACE SCIENCE

# The effect of interfacial energy and phase fraction on the particle shape and the dihedral angles in two-phase small particles containing a cusp-oriented interface; computational model

**A. M. Mebed · J. M. Howe**

Received: 28 April 2007 / Accepted: 18 June 2007 / Published online: 21 August 2007


**Abstract** The equilibrium shape and dihedral angles at the solid–liquid–vapor tri-junctions of two-phase alloy small particles containing a cusp-oriented interface were modeled as a function of phase fraction, surface energy and the interfacial energy. The calculation was applied to different combinations of surface and/or interfacial energies to demonstrate the various possible particle shapes and dihedral angles that result for two-phase particles. The dihedral angles at the tri-junction vary with the phase fraction, due to the coupling between the relative amounts of each phase, interfacial energy relative to the two surface energies and the equilibrium conditions at the tri-junction. These features can be used to find the ratio of the interfacial energy to the surface energies of two-phase particles for any state of matter.

## Introduction

It is well known that the balance between the surface and interfacial energy densities determines the resulting equilibrium dihedral angles at a three-phase junction (or tri-junction) [1–5]. This situation was illustrated in our previous paper [6]. These calculations are commonly used in the evaluation of wetting experiments [3–5]. In practice, the dihedral angles at a tri-junction are measured experimentally and then used to determine the grain boundary or interfacial energy, given known values for the surface energies of the phases. The dihedral angles need not be uniquely determined when one of the interfaces is cusp-oriented. Hoffman and Cahn [7, 8] showed that the force balance leading to the conditions for thermodynamic equilibrium applicable to a three-phase junction composed of anisotropic interfaces can be replaced by an inequality which eliminates one of the constraints on the dihedral angles. As a result, it should be possible for an equilibrium three-phase junction in which one interface is cusp-oriented to exhibit a range of dihedral angles. This situation has been discussed in detail recently with respect to grain boundaries [9].

In recent transmission electron microscope (TEM) investigations of two-phase Ag–Cu alloy nanoparticles [6], we observed large variations in the particle shapes and corresponding three-phase junction angles that appeared consistent with the surface/interfacial-energy balance predictions of Hoffman and Cahn [7]. In particular, the observed dihedral angles appeared to depend on the relative phase-fractions of the Cu-rich and Ag-rich phases. Similar variations of the dihedral angle on phase fraction have been recently reported for GaAs–GaSb nano ice-cream cones [10].

In this article, we present a simple, but powerful analytical calculation which shows that the balance among the surface and interfacial energy densities at the cusp-oriented interface between the two phases and the resulting dihedral angles depend on the relative phase fractions of the solid phases. This result has particularly important implications in nanostructured materials, where phase volumes are small

A. M. Mebed (✉)
Physics Department, Faculty of Science, Assuit University, Assuit 71516, Egypt
e-mail: abdu_55@yahoo.com

*Present Address:*
A. M. Mebed
Al-Jouf University, Skaka 2014, Kingdom of Saudi Arabia

J. M. Howe
Department of Materials Science and Engineering, University of Virginia, Charlottesville, VA 22904-4745, USA

and particles are often able to obtain their equilibrium shape. It also presents a new method to determine the relative values of the surface and interfacial energy densities in two-phase systems, based on the variation of the dihedral angles at the three-phase junction with phase fraction.

## Computational model

In this section, the equations specifying the equilibrium shape of a two-phase solid–liquid small particle in contact with its vapor and the corresponding boundary conditions for the equilibrium angles at the tri-junction containing an interface with a fixed orientation are obtained as a function of the relative amounts of each phase using variational calculus.

The solid–vapor and liquid–vapor surface energy densities ($\gamma_{SV}$ and $\gamma_{LV}$) are assumed to be isotropic while the solid-liquid interface is assumed to be cusp-oriented with interfacial energy density $\gamma_{LS}$. Interfacial and surface-stress effects are neglected and the composition fields within each phase are assumed homogeneous. These conditions imply that the phase compositions are independent of particle size and alloy composition, and that the effect of segregation on the surface and interfacial energies is ignored. The equilibrium shape of the two-phase particle is that which minimizes the sum of the surface and interfacial energies for a given phase fraction of the two solid phases. It is assumed that the experimental system is sufficiently small that global equilibrium has been obtained.

Initially, a two-dimensional L–S–V. system is considered, as depicted in Fig. 1. The L–S. interface is constrained to lie along the *y*-axis. The *x*-axis is taken to be a mirror plane. With the assumption of global equilibrium, the morphology of each phase depends on the amounts of each phase present.

### Calculation of total energy

Let $E_L$ and $E_S$ be the energies of the L and S phases, respectively, and $E_{LS}$ be the energy of the interface between the S and L phases. $S_L$ and $S_S$ are the surface areas of the L and S phases and $S_{LS}$ is the interfacial area. $\gamma_L$ and $\gamma_S$ are the surface energies of the L and S phases and $\gamma_{LS}$ is the interfacial energy. $\theta_L$, $\theta_S$ and $\theta_V$ are the dihedral angles, as illustrated in Fig. 1. Using these notations, the total energy of the system can be written as: $E = E_L + E_S + E_{LS}$, where $E_L = \gamma_L S_L$, and similarly for the other energies.

To find $S_L$, the situation depicted in Fig. 1, of two truncated unequaled-size spheres in contact with each other, has to be considered. If $A_L$ and $A_S$ represent the surface areas formed by revolution of a curve y = f(x) about the x axis of the L and S phases, then the following two constraints apply [11]:

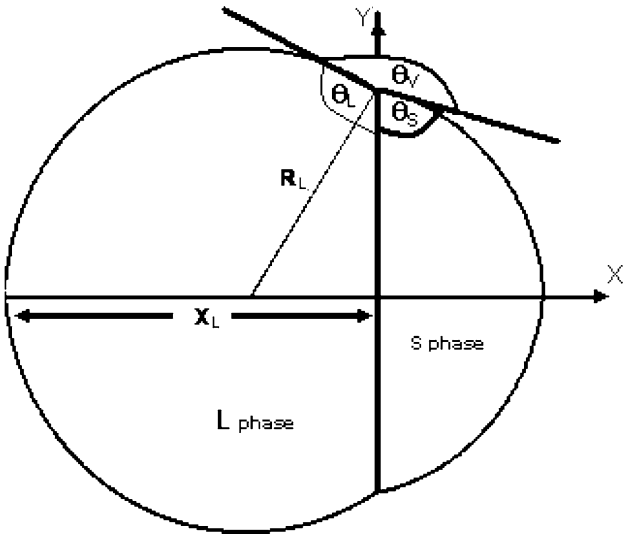


**Fig. 1** Cross-section of an equilibrium two-phase particle representing the solid L, S, and vapor V phases. The LS interface is cusp-oriented and constrained to lie along the y-axis

$$S_L = \int_0^{X_L} 2\pi y(x)\sqrt{1+\left(\frac{dy}{dx}\right)^2}\,dx, \tag{1}$$

$$y(x) = [R_L^2 - (R_L - x)^2]^{1/2}, \tag{2}$$

where $R_L$ is the radius of the truncated phase L. Accordingly, $S_L$ can be written as:

$$S_L = 2\pi R_L \int_0^{X_L} dx = 2\pi R_L X_L. \tag{3}$$

Similarly, $S_S$ can be written as:

$$S_S = 2\pi R_S X_S. \tag{4}$$

Then the total energy of the system can be written as:

$$E = 2\pi R_L X_L \gamma_L + 2\pi R_S X_S \gamma_S + \pi\gamma_{LS}(2R_L X_L - X_L^2). \tag{5}$$

### Volume of truncated sphere-like particles

The volume of the L sphere is given by [11]:

$$V_L = \int_0^{X_L} \pi y^2(x)dx = \pi X_L^2\left(R_L - \frac{X_L}{3}\right). \tag{6}$$

Likewise, the volume of the S sphere is given by:

$$V_S = \pi X_S^2\left(R_S - \frac{X_S}{3}\right). \tag{7}$$

$R_L$ and $R_S$ are estimated from Eqs. 6 and 7 to give the constraints:

$$R_L = \frac{V_L}{\pi X_L^2} + \frac{X_L}{3} \tag{8}$$

$$R_S = \frac{V_S}{\pi X_S^2} + \frac{X_S}{3}. \tag{9}$$

## Problem statement

The total energy E must be minimized subjected to the constraints in Eqs. 8 and 9 to give:

$$E = 2\pi X_L\gamma_L\left[\frac{V_L}{\pi X_L^2} + \frac{X_L}{3}\right] + 2\pi X_S\gamma_S\left[\frac{V_S}{\pi X_S^2} + \frac{X_S}{3}\right] + \pi X_L\gamma_{LS}\left[\frac{2V_L}{\pi X_L^2} + \frac{2X_L}{3} - X_L\right]. \tag{10}$$

Equation 10 is simplified to:

$$E = \frac{2V_L}{X_L}(\gamma_L + \gamma_{LS}) + \frac{\pi X_L^2}{3}(2\gamma_L - \gamma_{LS}) + \frac{2V_S\gamma_S}{X_S} + \frac{2\pi}{3}X_S^2\gamma_S. \tag{11}$$

The constraints $y(X_L) = y(X_S)$ using Eqs. 8 and 9 give:

$$\frac{2V_L}{X_L} - \frac{\pi}{3}X_L^2 - \frac{2V_S}{X_S} + \frac{\pi}{3}X_S^2 = 0. \tag{12}$$

Accordingly, the extrema occur when:

$$X_L = \left(\frac{3V_L}{\pi}\right)^{1/3}\frac{(\gamma_L + \gamma_{LS} - \lambda)^{1/3}}{(2\gamma_L - \gamma_{LS} + \lambda)^{1/3}} \tag{13}$$

and

$$X_s = \left(\frac{3V_S}{\pi}\right)^{1/3}\frac{(\gamma_S + \lambda)^{1/3}}{(2\gamma_S - \lambda)^{1/3}}, \tag{14}$$

where $\lambda$ is the Lagrange multiplier. To find $\lambda$, we use the remaining constraint condition in Eq. 12 with Eqs. 13 and 14, yielding:

$$\left(\frac{\pi}{3}\right)^{1/3}\left[2V_L^{2/3}\left(\frac{2\gamma_L - \gamma_{LS} + \lambda}{\gamma_L + \gamma_{LS} - \lambda}\right)^{1/3} - V_L^{2/3}\left(\frac{\gamma_L + \gamma_{LS} - \lambda}{2\gamma_L - \gamma_{LS} + \lambda}\right)^{2/3} - 2V_S^{2/3}\left(\frac{2\gamma_S - \lambda}{\gamma_S + \lambda}\right)^{1/3} + V_S^{2/3}\left(\frac{\gamma_S + \lambda}{2\gamma_S - \lambda}\right)^{2/3}\right] = 0. \tag{15}$$

Letting $\left(\frac{V_S}{V_L}\right)^{2/3} = g$, the phase fraction ratio, gives:

$$\left[2\left(\frac{2\gamma_L - \gamma_{LS} + \lambda}{\gamma_L + \gamma_{LS} - \lambda}\right)^{1/3} - \left(\frac{\gamma_L + \gamma_{LS} - \lambda}{2\gamma_L - \gamma_{LS} + \lambda}\right)^{2/3} - 2g\left(\frac{2\gamma_S - \lambda}{\gamma_S + \lambda}\right)^{1/3} + g\left(\frac{\gamma_S + \lambda}{2\gamma_S - \lambda}\right)^{2/3}\right] = 0. \tag{16}$$

Equation 16 can be written in the form of Eq. 17 giving a sextic polynomial in $\lambda$:

$$(\gamma_L - \gamma_{LS} + \lambda)^3(\gamma_S + \lambda)(2\gamma_S - \lambda)^2 - g^3(\gamma_S - \lambda)^3 \times (\gamma_L + \gamma_{LS} - \lambda)(2\gamma_L - \gamma_{LS} + \lambda)^2 = 0. \tag{17}$$

A simple computer program utilizing the Newton-Raphson method can be used to solve the above equation for $\lambda$, to find the roots to use in calculating both $X_L$ and $X_S$, and accordingly, $R_L$ and $R_S$, respectively.

## Special cases

i) If $\gamma_L = \gamma_S = \gamma_{LS} = \gamma$, Eq. 17 becomes:

$$(\gamma + \lambda)(2\gamma - \lambda)\left\{\lambda^3(2\gamma - \lambda) - g^3(\gamma - \lambda)^3(\gamma + \lambda)\right\} = 0. \tag{18}$$

Solutions including $\lambda = -\gamma$ and $\lambda = 2\gamma$ are not realistic, as they imply $V_L = 0$ or $V_s = 0$.

ii) If $\gamma_L = \gamma_S$ and $\gamma_{LS} = 0$, then:

$$(\gamma + \lambda)^4(2\gamma - \lambda)^2 - g^3(\gamma - \lambda)^4(2\gamma + \lambda)^2 = 0. \tag{19}$$

It is easy to note that $\lambda = 0$ is a solution for $g = 1$.

## Dihedral angles

It is straightforward to find the dihedral angles at a tri-junction from the calculations above. They are connected to the surface and interfacial energies by the relation:

$$\gamma_{LV}\cos\theta_L + \gamma_{SV}\cos\theta_S + \gamma_{LS} = 0. \tag{20}$$

## Results

There are many different combinations of surface and/or interfacial energies that can be used to demonstrate the various possible particle shapes and dihedral angles that result for two-phase particles. Here we present only a few of the possibilities to illustrate typical behavior.

Increasing the interfacial energy relative to the two surface energies

Figures 2a–c show the effect of increasing the interfacial energy on the equilibrium two-phase particle shape. The equilibrium particle shape was calculated from Eq. 17 for three different interfacial energies with the same value of the phase fraction ratio, $g$, of 0.4. For purposes of illustration, the figures were determined using the ratios of the surface energies of a real two-phase solid–solid system consisting of solid Co and Cu, i.e., 2550 and 1850 mJ/m$^2$, respectively [5]. In keeping with the notation of Fig. 1, we will refer to the two solid phases as L and S. Figure 2(d) shows the contact angles for this particle over the range of varying interfacial energy from 400 to 3500 mJ/m$^2$.

Figure 2a shows a situation where the L and S phases have the surface energies above, but $\gamma_{LS.}$ has its minimum value of 400 mJ/m$^2$. In this case, the particle is nearly spherical because the lower interfacial energy allows the particle to increase the relative proportion of interfacial area. Notice that $\theta_V$ is about 180$^\circ$ for this case in Fig. 2d.

It is useful to compare Fig. 2c with Fig. 2a. One can see that the particle in Fig. 2c adjusts its shape to compensate the increase in $\gamma_{LS}$ by shortening the length of the L–S interface and thereby increasing $\theta_L$ considerably. Figures 2a–c clearly show that the degree of puckering at the three-phase junction and hence, $\theta_V$, strongly depends on the interfacial energy, with low values of interfacial energy leading to little puckering. This feature can be used to estimate the relative magnitude of the interfacial energy compared to the surface energies of the two phases.

As might be expected, it was observed that increasing the interfacial energy relative to the two surface energies causes the particle to decrease the area of the L–S interface, thereby increasing the degree of puckering at the three-phase junction. This leads to smaller values of $\theta_V$ and larger values of $\theta_L$ and $\theta_S$, as shown in Fig. 2d. These variations can cause $\theta_V$ to lie above or below $\theta_L$ and $\theta_S$ on a plot such as Fig. 2d, depending on the ratios of the surface energies to the interfacial energy. Conversely, decreasing the interfacial energy increases the interfacial area, causing the particle to become more spherical, with the angles adjusting accordingly. In the limiting case where the interfacial energy approaches zero and the L and S phases have equal surface energies and phase fractions, the two-phase particle becomes spherical. This result is plotted in Fig. 3.

Effect of phase fraction

Figures 4a–d show the effect of the phase fraction on the equilibrium particle shape. In this calculation, the free energies of the L and S phases were taken as A = B = 1850 mJ/m$^2$ and the interfacial energy C = 300 mJ/m$^2$.

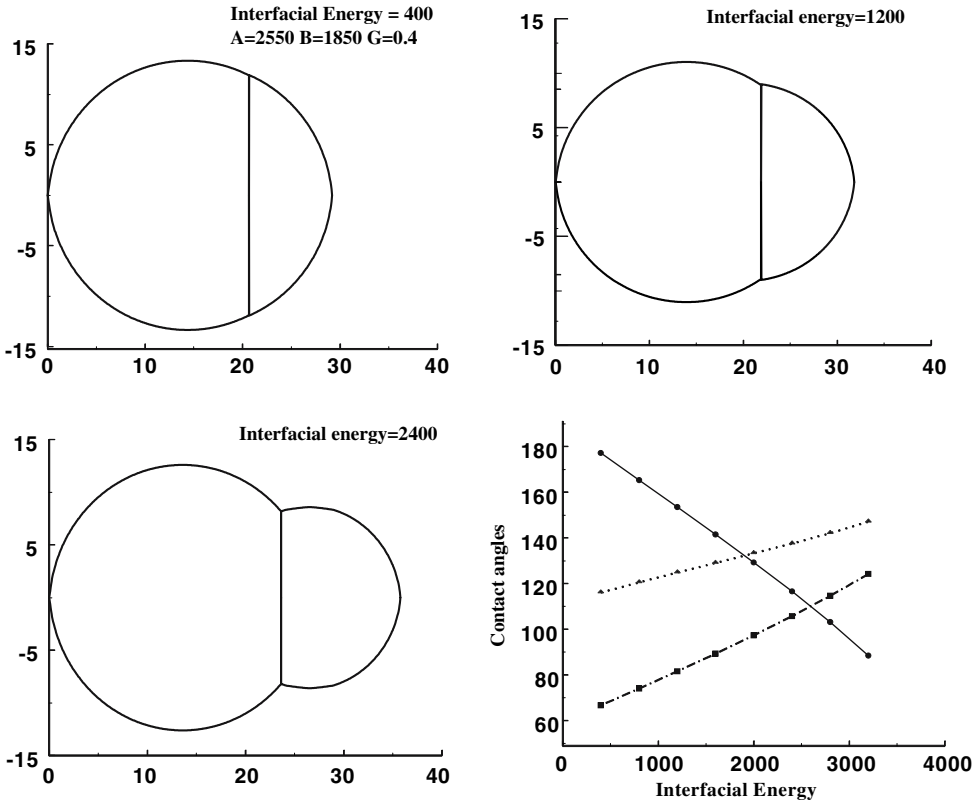


**Fig. 2** (**a**–**c**) Equilibrium particle shapes calculated as a function of the interfacial energy for a constant phase fraction ratio g = 0.4, and (**d**) graph of the contact angles for these and other particles over the range of interfacial energy from 400 to 3500. Solid line is for $\theta_V$, dotted line is for $\theta_L$ and dashed-dotted line is for $\theta_S$. All are calculated at the same values of the volume fraction. A and B are the surface energies for the L and S phases, respectively

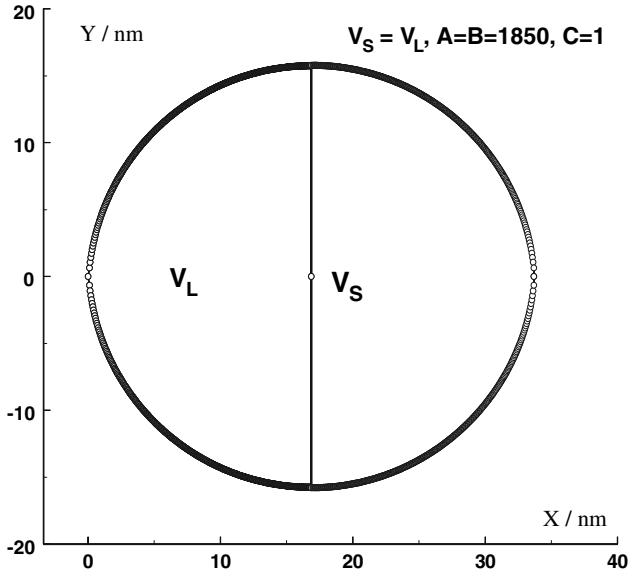


**Fig. 3** The interface of equilibrium two-phase particle calculated for the same volume fraction, surface energies A = B = 1850 with interfacial energy C as low as 1

Figures 4a–c present only a few of the possibilities to illustrate typical behavior of the particle shape as a function of the phase fraction ratio $g$ = 0.05, 0.4 and 0.8. The change in particle shape is clearly recognizable in this figure. Figure 4d shows a graph of the contact angles for these particles over the range of phase fraction ratio from 0.05 to 0.9. Note that $\theta_S$ steadily increases with increasing fraction of phase S over the range shown, while $\theta_L$ steadily decreases and $\theta_V$ gradually increases over the same range of phase fraction S. The behavior of the angles versus phase fraction in Fig. 4d is distinctly different from the behavior versus the interfacial energy shown in Fig. 2d. If there was no dependence of the dihedral angles on the phase fractions, the graph in Fig. 4d would consist of three horizontal lines with the values of $\theta_S$, $\theta_L$ and $\theta_V$ determined from the values of the surface and interfacial energies only.

## Effect of a high value of the interfacial energy

In contrast to the previous case (Fig. 4), where the interfacial energy was 300 mJ/m$^2$, the interfacial energy was increased to 3000 mJ/m$^2$ with the surface energies of the S and L phases held constant at 1850 mJ/m$^2$ in Fig. 5. A value of 3000 mJ/m$^2$ is thus nearly equal to the sum of the surface energies of the L and S phases and is thus, the maximum value one can expect for the interface [5]. Increasing the interfacial energy causes a dramatic change

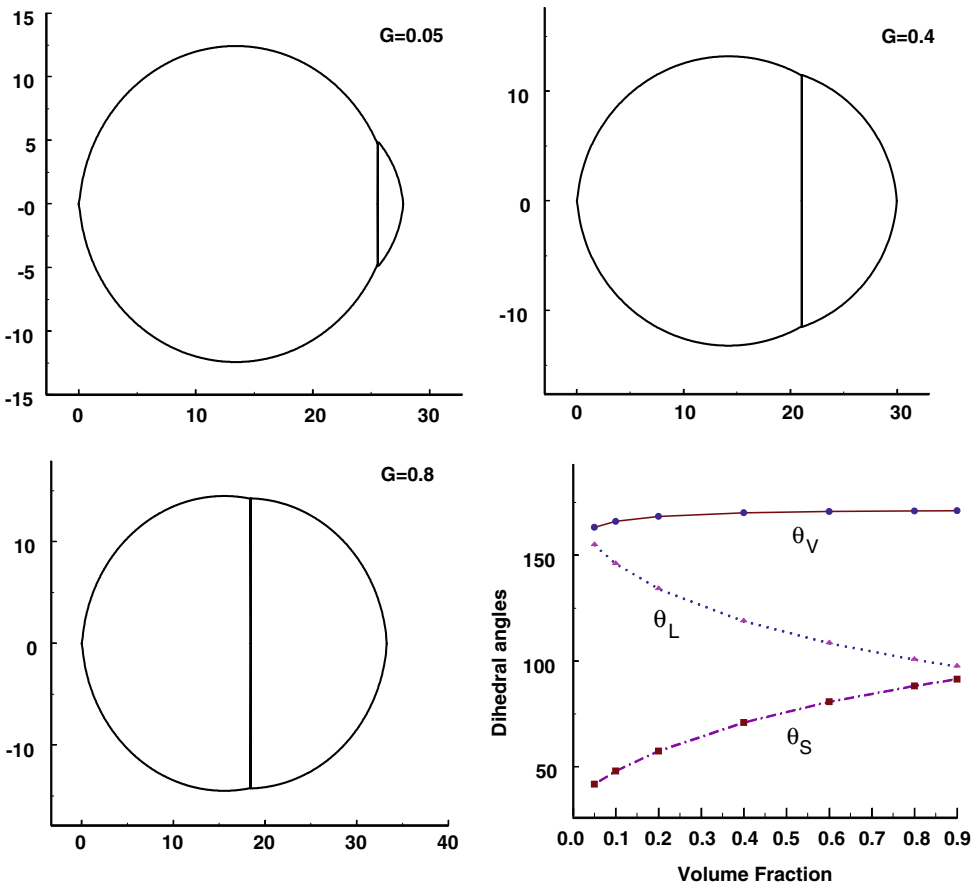


**Fig. 4** (**a**)–(**c**) Equilibrium particle shapes calculated as a function of the volume fraction G, and (**d**) graph of the contact angles for these and other particles over the range of volume fraction from 0.05 to 0.9. All are calculated at the same values of surface and interfacial energies. The particle diameter is in nanometers

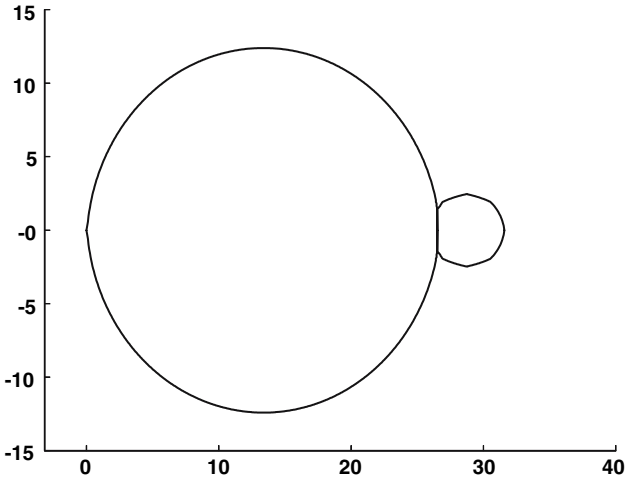


**Fig. 5** Equilibrium two-phase particles shape calculated for the same surface energy of 1850 mJ/m$^2$, a large interfacial energy of 3000 mJ/m$^2$, and a volume fraction ratio of 0.05. The X and Y dimensions are in nanometers

in the particle shape as well as the dihedral angles. This is seen in Fig. 5, where the two phases almost tend to exist as two separate spheres.

Figure 6 shows additional plots of the variation in dihedral angles with phase fraction for an interfacial energy of 3000 mJ/m$^2$, with the curves for $\theta_S$ and $\theta_L$ now lying substantially above that for $\theta_V$. This behavior occurs because the high value of $\gamma_{LS}$ produces a deep cusp at the tri-junction, thereby decreasing $\theta_V$ considerably, and correspondingly increasing both $\theta_S$ and $\theta_L$.

When Fig. 4d is compared to Fig. 6, it is seen that decreasing the L–S interfacial energy causes the curves for $\theta_S$ and $\theta_L$ to move apart and change in an almost

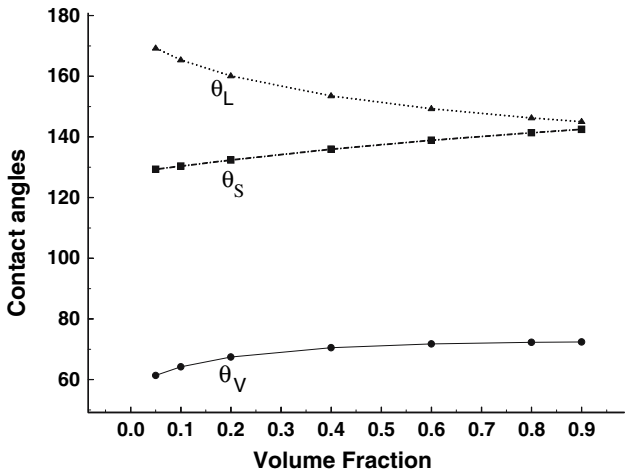


**Fig. 6** Graph of the contact angles for two-phase particles calculated over ranges of volume fraction from 0.05 to 0.9. All are calculated for the same surface energies and interfacial energies of 3000 mJ/m$^2$

complementary manner with phase fraction, while $\theta_V$ remains nearly constant over the range of phase fraction ratio $g$ from 0.1 to 0.9. This behavior is caused by the weak influence of the L–S interface on the resulting dihedral angles and nearly spherical shape of the two-phase particles.

## Discussion

The equilibrium calculations demonstrate that the dihedral angles at a three-phase junction vary with the volume fraction of the phases for spherical two-phase particles, when one interface (in this case the L–S interface) is cusp-oriented. In the absence of a cusp-oriented interface, the dihedral angles of a tri-junction are uniquely determined if the tri-junction is in thermodynamic equilibrium. If the surface and interfacial energy densities are independent of the normal, the various isotropic surfaces will possess constant, but different, curvatures at equilibrium, depending on the relative amounts of the phases present.

When one interface becomes cusp-oriented, there exists only one equilibrium condition at the tri-junction and a degree of freedom is introduced in the selection of the dihedral angles. Since the shape of the surfaces depends on the relative amounts of the phases [14], it is to be expected that the dihedral angles will also show a dependence on the phase fraction. A similar dependence of two of the dihedral angles on phase fraction should also exist when there are two cusp-oriented interfaces present in the tri-junction. In this case, there are no surfaces or interfaces that are parallel, the orientation is fixed only for the L–S interface, and the values of the dihedral angles $\theta_L$, $\theta_S$ and $\theta_V$ all depend on the phase fraction. The surfaces of both the L and S phases change orientation as the phase fractions change. The two undetermined angles provide a degree of freedom that must be solved simultaneously with the equilibrium conditions for the surfaces, again yielding a dependence of the two dihedral angles on the phase fraction.

In the case of solid phases, area fractions of phases measured experimentally may not be those of perfectly spherical particles due to faceting (see e.g., [6]). This difference can introduce some error between experimental measurements and calculations based on perfect spheres, i.e., assuming isotropic surface energies, but the qualitative behavior does not change. The situation of one cusp-oriented interface may be important in grain growth, where one grain-boundary may be cusp-oriented, e.g., containing a {111} plane or {111} twin boundary [7, 9, 12, 13]. In this case, the curvature and mobility of this grain boundary may be markedly different from the other grain boundaries at the tri-junction, which can change their dihedral angles, thereby facilitating grain boundary motion.

The present case is different than the classic 'sessile drop' experiment [2–5] with a liquid (or solid) droplet on a semi-infinite solid surface. In this case, the L–S. and S–V interfaces are the same and parallel. The angle $\theta_L$ does not vary with fraction of phase L, but the drop simply increases its size. In this case, there is no phase fraction dependence and the classic force balances discussed in references [1–5] apply.

The behavior described herein was for two metallic phases in equilibrium with their vapor, but similar behavior is expected to occur for other combinations of materials and states of matter, as evidenced by the example of grain boundaries mentioned above. Certain factors such as a strong orientation dependence of the surface and interfacial energies, i.e., anisotropy, may change the actual equilibrium angles quantitatively, but the same qualitative dependence on the phase fraction of material is anticipated.

It is worth mentioning than, interface facet could develop neighboring orientations in a real, unconstrained system [15], which is not considered in the present paper. The calculation of the interfacial Wulff shape being a cylinder, with its facet oriented in the Y direction, accordingly, calculating the limit of applicability of our model and characterizing the "bent-interface" solutions are in progress.

## Conclusions

The computational calculations in this study support the following conclusions:

1. The dihedral angles at the three-phase junction formed by two surfaces and a cusp-oriented interface are functions of the phase fraction.
2. Low values of the interfacial energy causes the dihedral angles $\theta_S$ and $\theta_L$ to move apart and change in an almost complementary manner with phase fraction ratio, with $\theta_V$ remaining above $\theta_S$ and $\theta_L$ and nearly constant over the range of phase fraction. In contrast, a high value of the interfacial energy causes the dihedral angles, with the curves for $\theta_S$ and $\theta_L$, to lie substantially above that for $\theta_V$.
3. The relative ratio of the interfacial energy to the surface energies for two-phase particles can be estimated from the degree of puckering at the tri-junction. The dependence of the tri-junction angles on phase fraction allows the ratios of the surface and interfacial energy densities to be determined experimentally using the tri-junction equilibrium conditions.

**Acknowledgements** The authors gratefully acknowledge support by the National Science Foundation under Grant DMR-0554792 (JMH). The authors also gratefully acknowledge the great contributions and valuable discussions with professor W. C. Johnson (AMM).

## References

1. Herring C (1951) In: Kingston WE (ed). The physics of powder metallurgy. McGraw-Hill, New York, p 143
2. Young T (1805) Philos Trans Roy Soc Lond 95:65
3. Adamson AW (1967) Physical chemistry of surfaces. 2nd Ed. Wiley, New York
4. Murr LE (1975) Interfacial phenomena in metals and alloys. Ch 2. Addison-Wesley, Reading MA, p 3
5. Howe JM (1997) Interfaces in materials: atomic structure, thermodynamics and kinetics of solid–vapor, solid–liquid and solid–solid interfaces. Wiley, New York, pp 179–83
6. Howe JM, Mebed AM, Chatterjee K, Li P, Murayama M, Johnson WC (2003) Acta Mater 51:1359
7. Hoffman DW, Cahn JW (1972) Surf Sci 31:368
8. Cahn JW, Hoffman DW (1974) Acta Metall 22:1205
9. King AH (1998) In: Weiland H, Adams BL, Rollett AD (eds). Grain growth in polycrystalline materials III. The Minerals, Metals and Materials Society, Warrendale, p 333–338.
10. Schamp CT, Jesser WA (2005) In: Howe JM, Laughlin DE, Lee JK, Dahmen U, Soffa WA (eds). Solid-Solid Phase Transformations in Inorganic Materials, vol 2. The Minerals, Metals and Materials Society, Warrendale, pp 1089–1100
11. Belding WG (ed) (1983) ASM handbook of engineering mathematics. American Society for Metals, Metals Park, p 161
12. Koo JB, Yoon DY (2001) Metall Mater Trans 32A:1911
13. Lee SB, Yoon DY, Henry MF (2000) Acta Mater 48:3071
14. Chatain D, Wynblatt P, Hagege S, Siem E, Carter C (2001) Interface Sci 9:191
15. Siem EJ, Carter WC (2004) Dominique Chatain, Phill Mag 84(10):991